Talanta 206 (2020) 120180

Contents lists available at ScienceDirect

Talanta

journal homepage: www.elsevier.com/locate/talanta

Ultrasonic-assisted extraction and digestion of proteins from solid biopsies followed by peptide sequential extraction hyphenated to MALDI-based profiling holds the promise of distinguishing renal oncocytoma from chromophobe renal cell carcinoma

Susana Jorge[a,b], Kevin Pereira[b], Hugo López-Fernández[c,d,e,f,g], William LaFramboise[h,1], Rajiv Dhir[h], Javier Fernández-Lodeiro[a,b], Carlos Lodeiro[a,b], Hugo M. Santos[a,b], Jose L. Capelo-Martínez[a,b,*]

[a] LAQV, REQUIMTE, Departamento de Química, Faculdade de Ciências e Tecnologia, Universidade NOVA de Lisboa, 2829-516, Caparica, Portugal
[b] PROTEOMASS Scientific Society, Madan Park, Rua dos Inventores, 2825-152, Caparica, Portugal
[c] ESEI –Escuela Superior de Ingeniería Informática, Edificio Politécnico, Campus Universitario As Lagoas s/n, Universidad de Vigo, 32004, Ourense, Spain
[d] CINBIO –Centro de Investigaciones Biomédicas, University of Vigo, Campus Universitario Lagoas-Marcosende, 36310, Vigo, Spain
[e] SING Research Group, Galicia Sur Health Research Institute (IIS Galicia Sur), SERGAS-UVIGO, Hospital Álvaro Cunqueiro, 36312, Vigo, Spain
[f] Universidade do Porto, Rua Alfredo Allen, 208, 4200-135, Porto, Portugal
[g] Instituto de Biologia Molecular e Celular (IBMC), Rúa Alfredo Allen, 208, 4200-135, Porto, Portugal
[h] Department of Pathology, University of Pittsburgh Medical Center, Pittsburgh, PA, United States

ARTICLE INFO

Keywords:
Renal oncocytoma
Chromophobe renal cell carcinoma
Renal cancer
MALDI
Profiling ESI
Sequential extraction

ABSTRACT

A novel analytical approach is proposed to discriminate between solid biopsies of chromophobe renal cell carcinoma (chRCC) and renal oncocytoma (RO). The method comprises the following steps: (i) ultrasonic extraction of proteins from solid biopsies, (ii) protein depletion with acetonitrile, (iii) ultrasonic assisted in-solution digestion using magnetic nanoparticle with immobilized trypsin, (iv) C18 tip-based preconcentration of peptides, (v) sequential extraction of the peptides with ACN, (vi) MALDI-snapshot of the extracts and (vii) investigation of the extract containing the most discriminating features using high resolution mass spectrometry. With this approach we have been able to differentially cluster renal oncocytoma and chromophobe renal cell carcinoma and identified 18 proteins specific to chromophobe and seven unique to renal oncocytoma. Chromophobes express proteins associated with ATP function (ATP5I & 5E; VATE1 & G2; ADT2), glycolysis (PGK1) and neuromedin whilst oncocytomas express ATP5H, ATPA, DEPD7 and TRIPB thyroid receptor interacting protein.

1. Introduction

Renal cell carcinoma is the 12th most frequently diagnosed cancer worldwide with 5% classified as chromophobe renal cell carcinoma (chRCC) which requires therapeutic radical or partial nephrectomy. Diagnosis of chRCC is complicated by morphological and histological features that overlap with renal oncocytoma (RO), a benign neoplasm that occurs at a similar frequency (5%) but has a positive prognosis and does not require aggressive treatment. For instance, staining for CD117, which is used to distinguish chRCC from other malignant subtypes of RCC, is helpless to discriminate chRCC of RO. As another example, when staining is done with cytokeratin 7 (CK7), a diffuse staining pattern in presented in chRCC with pale cells. Yet, in the eosinophilic variant of chRCC, CK7 staining is limited and very similar to RO [1–3]. Despite the efforts to find biomarkers to distinguish these two tumors, a unique pattern for each one remains to be undisclosed. Therefore, there is an urgent need for new methods that can effectively differentiate between these renal neoplasms.

* Corresponding author. LAQV, REQUIMTE, Departamento de Química, Faculdade de Cieˆncias e Tecnologia, Universidade NOVA de Lisboa, 2829-516, Caparica, Portugal.
E-mail address: jlcm@fct.unl.pt (J.L. Capelo-Martínez).
[1] Present Addresses: Chief Genomics Technology Officer, Allegheny Health Network, Allegheny Cancer Institute, Allegheny General Hospital-O242B, 320 East North Avenue, Pittsburgh, PA 15212.

https://doi.org/10.1016/j.talanta.2019.120180
Received 11 May 2019; Received in revised form 22 July 2019; Accepted 24 July 2019
Available online 27 July 2019
0039-9140/

Abbreviations

Ambic	Ammonium bicarbonate
APS	Ammonium persulphate
ATP	Adenosine triphosphate
ATP5E	ATP synthase subunit epsilon, mitochondrial
ATP5H	ATP synthase subunit d, mitochondrial
ATP5I	ATP synthase subunit e, mitochondrial
ATPA	ATP synthase subunit alpha, mitochondrial
chRCC	Chromophobe renal cell carcinoma
CK7	Cytokeratin 7
DEPD7	DEP domain-containing protein 7
FA	Formic acid
HR	High resolution
IAA	Iodoacetamide
NAT	Normal adjacent tissue
OCT	Optimal cutting temperature
PGK1	Phosphoglycerate kinase 1
RCC	Renal cell carcinoma
RO	Renal oncocytoma
TCA	Trichloroacetic acid
TOF	Time of flight
TRIPB	Thyroid receptor-interacting protein 11
VATE1	V-type proton ATPase subunit E 1
VATG2	V-type proton ATPase subunit G 2
α-CHCA	α-cyano-4-hydroxy-cinnamic acid

In biomedical research, sample treatment is considered a bottleneck in analysis due the large number of steps needed to make the samples ready for analysis. To overcome this problem, diverse extraction techniques, including solid-phase extraction (SPE), liquid-liquid extraction (LLE), or protein precipitation, have been used in sample preparation of biomolecules of interest. Moreover, extraction procedures are currently used in biomedical analysis and research to simplify the matrix, clean-up the sample and/or selectively enrichment of a given analyte [4–10]. Among these extraction procedures, on-a-tip SPE strategies has been widely applied in the proteomic field, specially C18 resin packed on-a-tip. Thus, the sequential extraction of peptides with C18-based tips has been used to reduce proteome complexity of biological samples through sequential extraction of peptides followed by mass spectrometry interrogation with the aim of finding biomarkers of diseases [11]. Taking into consideration the problems and solutions described above, a methodology to elucidate differences between chromophobe renal cell carcinoma and renal oncocytoma has been developed as follows. First, the sample treatment is optimized to reduce proteome complexity using ultrasonic assisted protein extraction from solid biopsies. The substrates then undergo (i) protein depletion with acetonitrile, ACN, (ii) ultrasonic assisted in-solution digestion using magnetic nanoparticle with immobilized trypsin, (iii) peptide preconcentration with C18-tips and (iv) peptide sequential extraction with ACN [13–15]. Finally, MALDI mass spectrometry was employed to provide a snapshot of the tumor proteomes revealing the most discriminative features specific to chRCC versus RO. The extracts were further investigated using nano-HPLC and high-resolution mass spectrometry (nano-LC-HR-MS). This tool may be extended to any disease presenting similar pathological profiles but with different outcomes. The method here presented can be extended to large cohort of samples using the high throughput provided by the 96-well plate-based ultrasonic approach [12], thus holding the promise of being used in routine medical assays.

2. Materials and methods

2.1. Reagents

All reagents used were HPLC or electrophoresis grade. Coomassie brilliant blue G-250, urea, albumin from bovine serum (BSA), Bradford reagent, iodoacetamide (IAA), ammonium dihydrogen-phosphate ($NH_4H_2PO_4$), N,N,N',N' – tetramethylethylene diamine (TEMED), and trichloroacetic acid (TCA) were purchased from Sigma-Aldrich (Basel, Switzerland). Ammonium bicarbonate (Ambic), α-cyano-4-hydroxy-cinnamic acid (α-CHCA) were purchased from Fluka (Basel, Switzerland). Trifluoroacetic acid (TFA) was purchased from Thermo Fischer Scientific (Waltham, MA, USA). Ammonium persulphate (APS) and tris base were purchased from NZYTech (Lisbon, Portugal). Acetonitrile (ACN) and formic acid (FA) were purchased from Carlo Erba Reagents (Val de Reuil, France). Dithiothreitol (DTT) and 4x Laemmli SDS sample buffer were purchased from Alfa Aesar (Karlsruhe, Germany). 10x tris/glycine/SDS running buffer and precision plus protein™ standards unstained were purchased from Bio-Rad (CA, USA). Pierce™ C18 tips, 100 µL bed were purchased from Thermo Fisher Scientific. Peptide calibration standard II from Bruker (Bremen, Germany) was used as a mass calibration standard for MALDI-TOF-MS measurements.

2.2. Material

Protein digestion was done in Eppendorf safe-lock tubes of 0.5 mL volume (Hamburg, Germany). A vacuum concentrator centrifuge model UNIVAPO 150 ECH Speed Vac and a vacuum pump model UNIJET II (Munich, Germany) were used for sample drying and sample pre-concentration. A mini incubator from Labnet (New Jersey, USA) was used for protein reduction steps. Vortex models ELMI CM70M-09 SkyLine (Southern California, USA), and Prism™ R refrigerated microcentrifuge, VX-200 Lab vortex mixer, AccuBlock™ digital dry baths from Labnet (New Jersey, USA), were used throughout the sample treatment. CLARIOstar® high performance monochromator multimode microplate reader from BMG LABTECH (Germany) was used for Bradford assays. Mini-PROTEAN tetra cell and PowerPac™ basic power supply from Bio-Rad (CA, USA) was used for SDS-PAGE protein separation. Image gels were obtained using a ProPic II gel imaging (Digilab-Genomic Solutions, USA). An ultrasonic processor UP50H (50 W, 30 kHz, 1 mm diameter probe tip) from Hielscher Ultrasonics (Teltow, Germany) was used for tissue homogenization. An ultrasonic bath, model TI-H-5, from Elma (Singen, Germany) with control of temperature and amplitude was used to sample cleaning and enhance protein depletion, and a sonoreactor model UTR200 from Dr.Hielscher (Teltow, Germany) was used to accelerate enzymatic digestions. Acquisition of mass spectrometry data was done using an Ultraflex II MALDI-TOF/TOF and an UHR-QqTOF IMPACT HD from Bruker Daltonics (Bremen, Germany). Chromatographic separation of peptides was carried out using an Ultimate 3000 nLC nano-system equipped with a trap-column Acclaim PepMap100, 5 µm, 100 Å, 300 µm i.d. × 5 mm (Thermo Fisher Scientific) and an analytical column Acclaim™ PepMap™ 100 C18, 2µm, 0.075mm i.d x 150mm (Thermo Fisher Scientific).

2.3. Kidney samples

The human kidney tissue samples were collected by the University of Pittsburgh Biospecimen Core's and the study was approved by the Institutional Review Board at the University of Pittsburgh (IRB # 02–077). All neoplasms contained a minimum of 90% tumor cells and NAT specimens were at least 90% normal cells. Data of patients enrolled in this study are summarized in Table 1.

2.4. Extracting proteins from kidney biopsies

The OCT-embedded tissues were treated as described in Jorge et al.

Table 1
Description of human kidney biopsies used in the study.

Sample	Age	Gender	Diagnosis[a]	Sample type[a]
N1	50–59	Male	RCC	NAT
N2	40–49	Female	Papillary	NAT
N3	50–59	Female	RCC	NAT
N4	70–79	Female	RCC	NAT
N5	70–79	Male	RCC	NAT
C6	70–79	Male	RCC	chRCC
C7	60–69	Female	RCC	chRCC
C8	70–79	Male	RCC	chRCC
C9	50–59	Female	RCC	chRCC
C10	80–89	Male	RCC	chRCC
O11	80–89	Male	RCC	RO
O12	60–69	Female	RCC	RO
O13	60–69	Male	RCC	RO

[a] RCC: renal cell carcinoma; NAT: normal adjacent tissue; chRCC: chromophobe renal cell carcinoma; RO: renal oncocytoma.

[16]. Initially washed with 2 ml of 70% (v/v) ethanol at 4 °C, submitted to ultrasound energy using an ultrasonic bath, 35 kHz, for 2 min, 100% amplitude, and centrifuged at 4 °C for 2 min (5,000 g). The supernatants were carefully removed, and the procedure was repeated. Cell pellets were then washed with 2 ml of water at 4 °C, sonicated again using an ultrasonic bath, 35 kHz for 2 min at 100% amplitude, and centrifuged at 4 °C for 2 min (5,000 g). Then, the supernatant was carefully removed, and the above steps were performed five times for each pellet. After OCT cleaning, each pellet was placed in a mortar and ground to a powder in liquid nitrogen using a pestle. The resulting powder was extracted for protein in 8 M urea/25 mM Ambic buffer (ratio: 100 µL buffer to 10 mg of tissue) using an ultrasonic processor UP50H (50 w, 30 kHz, 1 mm diameter probe tip) operating at 50% amplitude for 2 min in a pulsed mode, 10 s on/10 s off. The samples were centrifuged at 10,000 g for 10 min and the supernatants were transferred to new tubes. The ultrasonic extraction procedure was repeated for the pellets and the second supernatant was combined with the first to produce the final protein extract. Each protein extract was precipitated using the DOC/TCA and acetone method. Briefly, to each 300 µL of protein extract, 3 µL of 2% DOC were added and left on ice for 20 min, then 75 µL of 100% TCA were added to the mixture and the samples were left on ice for 20 min, followed by centrifugation at 4 °C for 20 min (16,000 g). The supernatant was removed, and the pellets were washed with 200 mL of ice-cold acetone (−20 °C), followed by centrifugation (16,000 g for 20 min at 4 °C). Then, 20 µL of 0.2 M NaOH were added to the protein pellet, and after 2 min at room temperature, 80 µL of 6 M urea in 25 mM Ambic were added. The proteins were solubilized using four cycles of 10 s ultrasound energy through an ultrasonic processor UP50H (50 w, 30 kHz, 1 mm diameter probe tip) operating at 50% amplitude. Finally, total protein content was determined using a Bradford protein assay. This extract was used further as described in the following sections.

2.5. ACN-based protein depletion

Protein depletion was assayed using extracts containing a total of 250 µg of proteins and two different ACN concentrations (v/v): (i) 20% or (ii) 45%. Each extract was prepared in triplicate. Then, samples were sonicated using an ultrasonic bath (35 kHz, 100%, 20 min) and the pellet formation was then observed after centrifugation at 14,000 g for 10 min, thus allowing the separation of the ACN-based precipitated proteins. Thus, two fractions for further study were obtained: the supernatant (SN) and the pellets. The SN fractions were evaporated to dryness.

2.6. SDS-PAGE

To perform the electrophoresis, dried SN samples were resuspended in 55,5 µL of Milli-Q H_2O plus 18.5 µL of 4x Laemmli SDS sample buffer, whilst the pellet was dissolved in 1.9 µL of 4x Laemmli SDS sample buffer plus 5.7 µL of Milli-Q water. Five µL of each sample were loaded on a 4% acrylamide/bis-acrylamide stacking gel and 12% acrylamide/bis-acrylamide running gel at 1mm of thickness. Additionally, 3 µL of molecular weight marker were also loaded. The gels were run at 200 V, and 400 mA during 50 min and then stained overnight with colloidal Coomassie blue. After staining, the gels were washed with Milli-Q water until a clear background was achieved. Gel imaging was carried out with a ProPic II-robot using 14 ms of exposure time and a resolution of 70 µm.

2.7. Protein quantification

Prior to quantification, samples were resuspended in equal amounts of Milli-Q water (184 µL) and then quantified using the Bradford protein assay. Briefly, a BSA standard curve (0, 0.2, 0.4, 0.6, 0.8, 1.0, 1.2, 1.4 µg/µL) was generated in duplicate. In duplicate wells, 5 µL of samples were mixed with 250 µL of Bradford reagent. The unknown samples were diluted with water to an approximate concentration between 0.4 and 1 µg/µL, then 5 µL of each unknown were mixed with 250 µL Bradford reagent. Finally, the samples were incubated at room temperature for 20 min, and the absorbances measured at 590 nm through a high-performance monochromator multimode microplate reader.

2.8. Reduction and alkylation

2.8.1. Supernatant

Supernatant fractions were prepared from 60 µg of extract in a volume of 88 µL so that the SN could later be split into 6 extracts. The pH of the samples was adjusted with 1 µL of 1 M Ambic, to a final concentration of 12.5 mM. Then, proteins were reduced with 9 µL of DTT (110 mM in 12.5 mM Ambic) and incubated at 37 °C for 1 h. The resulting cysteines were blocked with 9 µL of IAA (400 mM in 12.5 mM Ambic). Since iodoacetamide is light-sensitive, all tubes were kept in darkness for 45 min at room temperature. Free IAA was inactivated by adding 3 µL of DTT (110 mM in 12.5 mM Ambic) to each sample.

2.8.2. Pellet

The pellet fractions were also reduced and alkylated. Ten µg of total protein were prepared in a final volume 115 µL and 1.5 µL of 1 M Ambic was added to adjust the pH to a final concentration of 12.5 mM. Proteins were reduced with 12 µL of DTT (110 mM in 12.5 mM Ambic) and incubated at 37 °C for 1 h. The resulting cysteines were then blocked with 12 µL of IAA (400 mM in 12.5 mM Ambic) in the dark for 45 min at room temperature. Finally, free IAA was inactivated by adding 4 µL of DTT (110 mM in 12.5 mM Ambic) to each sample.

2.9. In-solution digestion of supernatants and pellets

In-solution digestion was performed using homemade magnetic nanoparticles with immobilized trypsin [17–19]. 20 µL of 3 mg/mL of immobilized trypsin were added to each sample, and the samples were digested using an ultrasonic sonoreactor device at 50% amplitude for 2 × 2.5 min with temperature constant at 20 °C. A magnet was subsequently used to immobilize the trypsin magnetic beads. The supernatant was transferred to new microtubes and evaporated to dryness.

2.10. Peptide sequential elution

The samples were resuspended after digestion in 50 µL of 0.1% (v/v) TFA and then loaded onto Pierce™ C18 tips with a 100 µL bed for

rapid sample desalting and concentrating peptides. First, C18 tips had to be activated by aspirating and dispensing five cycles of 50 µL of an 80% (v/v) ACN + 0,1% (v/v) TFA solution, and then 50 µL of a 0.1% (v/v) TFA solution (3 cycles) before sample pipetting. The peptides were retained in the C18 tips by aspirating and dispensing the samples 20 cycles. Finally, the C18 tips were washed with 50 µL of 0.1% (v/v) TFA twice to remove the salt content, and then were sequentially eluted with 50 µL of different ACN concentrations (4%, 7%, 10%, 14%, 35% and 60%) by aspirating and dispensing each concentration 15 cycles, from the lowest to highest concentration. All extracts were then evaporated to dryness.

2.11. Mass spectrometry

Samples were resuspended in 10 µL of 0.3% formic acid (v/v) for MS analysis and 0.5 µL of the sample was hand-spotted, in quintuplicate, onto a MALDI target plate. 1 µL of a matrix solution of 7 mg α-cyano-4-hydroxycinnamic acid was dissolved in 90 mM $NH_4H_2PO_4$, 50% (v/v) ACN and 0.1% (v/v) TFA was added and allowed to air dry. The MALDI TOF/TOF mass spectrometer was operated in positive ion mode using a reflectron, and spectra were acquired in the m/z range of 600–3500. A total of 500 spectra were acquired for each sample at a laser frequency of 50 Hz. External calibration was performed with the $[M + H]^+$ monoisotopic peaks of bradykinin 1–7 (m/z 757.3992), angiotensin II (m/z 1046.5418), angiotensin I (m/z 1296.6848), substance P (m/z 1758.9326), ACTH clip 1–17 (m/z 2093.0862), ACTH18– 39 (m/z 2465.1983) and somatostatin 28 (m/z 3147.4710).

2.12. Hierarchical clustering analysis

The corresponding raw data spectrum of each sample generated by the MS analysis was pre-processed with the Mass-Up v1.0.9 open source program (http://sing. ei.uvigo.es/mass-up/) [20] using the following parameters: (i) intensity transformation (squareroot), (ii) smoothing (none), (iii) baseline correction (snip), (iv) standardization (total ion current), (v) peak detection (MALDIquant: SNR (3), half window size (60) and (vi) minimum peak intensity (0.001). Peaks were matched with the following parameters: (i) intra-sample matching (MALDIquant: tolerance (0.002)), selecting the “generate consensus spectrum” box with a percentage of presence of 60%, (ii) inter-sample matching (MALDIquant: tolerance (0.002)). Then, an agglomerative, hierarchical clustering analysis was executed with the following parameters: (i) minimum variance (0.1), (ii) peak list (NULL > for no peak filtering), (iii) cluster reference value (average), (iv) distance function (hamming), (v) conversion values (presence), (vi) intra-sample minimum presence (0), (vii) deep clustering (No).

2.13. Nano-LC-HR-MS/MS analysis

The nanoLC-HR-MS/MS analysis was carried out using an Ultimate 3000 nLC nano-system coupled to an UHR-QqTOF IMPACT HD (Bruker Daltonics) with a CaptiveSpray ion source (Bruker Daltonics). All samples were reconstituted in 50 µL of 3% ACN/0.1% (v/v) aqueous formic acid. 5 µL of peptides were loaded into a trap column Acclaim PepMap100, 5 µm, 100 Å, 300 µm i.d. × 5 mm and desalted for 5 min with 3% of mobile phase B (B: 90% ACN 0.1% FA) at a flow rate of 15 µL/min. Chromatographic separation was carried out using an analytical column Acclaim™ PepMap™ 100 C18, 2 µm, 0.075 mm i.d x 150 mm with a linear gradient at 300 nL/min (mobile phase A: aqueous FA 0.1% (v/v); mobile phase B 90% (v/v) ACN and 0.08% (v/v) FA), 0–60 min from 3% to 35% of mobile phase B, 60–70 min linear gradient from 35% to 95% of mobile phase B, 70–80 min 95% B. Total run time was 100 min. For each sample, two replicate injections were performed. Chromatographic separation was carried out at 35 °C. MS acquisition was set to cycles of MS (2 Hz), followed by MS/MS (8–32Hz), cycle time 3.0 s, with active exclusion (precursors were excluded from precursor selection for 0.5 min after acquisition of 1 MS/MS spectrum, intensity threshold for fragmentation of 2500 counts). Together with active exclusion set to 1, reconsider precursor if the intensity of a precursor increases by a factor of 3, this mass will be taken from temporarily exclusion list and fragmented again, ensuring that fragment spectra were taken near to the peak maximum. All spectra were acquired in the range 150–2200 m/z. Raw data were processed in DataAnalysis 4.2 and subsequently exported to Protein-Scape 4.0 for automated protein identification. For protein identification, CID-MS2 spectra were first searched against the *H. sapiens* (20,266 sequences) subset of the SwissProt database 57.15 (515,203 sequences; 181,334,896 residues), using the Mascot search engine (V. 2.3.02) with the following parameters: (i) two missed cleavage; (ii) fixed modifications: carbamidomethylation (C); (iii) variable modifications: oxidation of methionine, Acetyl (Protein N-term), Glu- > pyro-Glu (N-term E), Gln- > pyro-Glu (N- term Q), (vi) peptide mass tolerance up to 20 ppm, (v) fragment mass tolerance 0.05 Da (vi) Adjust FDR 1%.

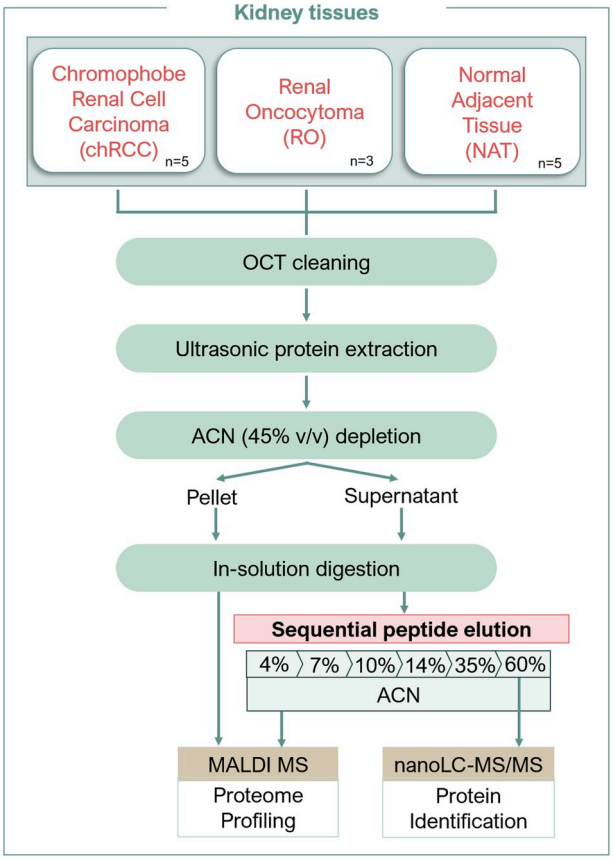

Fig. 1. The solid biopsies are cleaned with the aid of an ultrasonic bath. Then, the proteins are solid-liquid extracted with the aid of an ultrasonic probe. The proteins are depleted with ACN 45% v/v, and thus one supernatant and one pellet are obtained. The supernatant is withdrawn, then evaporated to dryness and then resuspended in 12.5 mM Ambic. The pellets were dissolved 12.5 mM Ambic. Proteins contained in supernatant and pellet were further reduced, alkylated and digested with the aid of ultrasonic energy. The peptides from the supernatant were then sequentially extracted using C18 tips and profiled using MALDI-based mass spectrometry. The best ACN fraction, 60% v/v was further interrogated using ESI-based mass spectrometry.

3. Results and discussion

Fig. 1 shows the comprehensive scheme used for the work presented herein.

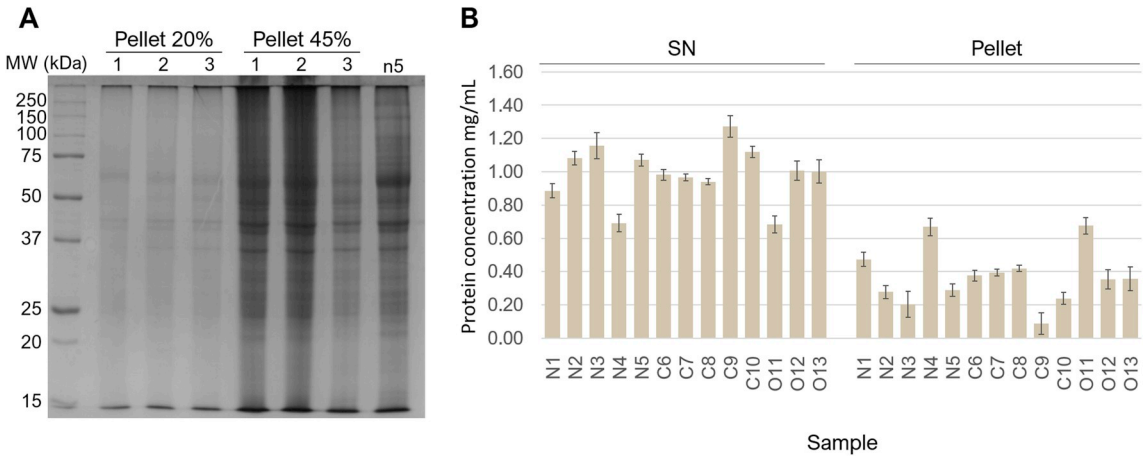

Fig. 2. (A): Influence of ACN concentration (v/v) on depletion of protein extracts from solid biopsies. SDS-PAGE of pellet fraction after protein depletion with (i) 20% and (ii) 45% (v/v) of ACN. Depletion was performed in triplicate (3 lanes for each ACN concentration) and N represents a crude protein extract without depletion. (B) Protein content of pellets and supernatants after depletion with 45% (v/v) ACN.

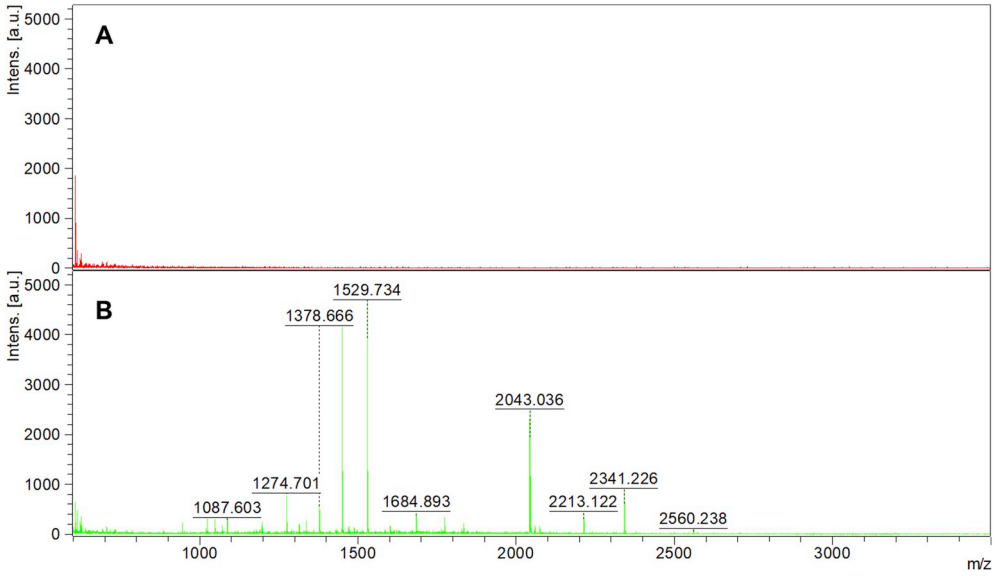

Fig. 3. Representative MALDI-MS spectra obtained for the 35% (v/v) ACN sequential fraction from (A) pellet and (B) supernatant. Note that the ACN 35% (v/v) pellet extract does not contain peptides.

3.1. Optimization of ACN concentration to simplify the proteome

We have previously shown that plasma samples depleted using ACN a supernatant reach in apolipoproteins is obtained [13]. The concentration of proteins of high molecular weight remaining in the supernatant decreases dramatically as the ACN concentration is increased. Conversely, the amount of high molecular weight proteins in the pellet increases. Because the samples used in this case were not plasma, but extracts obtained from tissue biopsies, we first performed a set of experiments to assess the effects of ACN on protein depletion. The ACN concentrations selected were 20% (v/v) and 45% (v/v) based on our experience with this sample treatment [13,21]. As can be seen in Fig. 2A, protein depletion with 45% (v/v) ACN concentration renders a pellet with higher concentration of proteins reflecting their depletion from the supernatant. We have previously established that clustering from the supernatant using MALDI-based mass spectrometry protein analysis is optimized after depletion of high molecular weight proteins plasma samples using ACN [13]. Therefore, we chose the ACN concentration of 45% (v/v) for further experiments.

3.2. Sequential elution of peptides

The sequential extraction of peptides using C18-based tips in conjunction with mass spectrometry has been previously described as a method to discriminate among large cohorts of samples [11,15]. We employed this approach on the (i) supernatants and (ii) pellets after depletion with 45% (v/v) ACN from (i) chromophobe renal cell carcinoma (chRCC) or (ii) renal oncocytoma (RO) or (iii) normal adjacent tissue (NAT). The proteomes were first digested with trypsin and then the peptides were up-loaded in C18 tips. The peptides were sequentially eluted with ACN solutions (% v/v: 4, 7, 10, 14, 35 and 60) based on our previous work with plasma [11].

Protein quantification of supernatants and pellets obtained after depletion with ACN 45% (v/v) concentration revealed that as much as 73% of the protein content remained in the supernatant. The total protein content of some pellets was too low for the sequential extraction procedure (see Fig. 2B). For example, sequential extractions of some digested pellets produced poor MALDI spectra, e.g. low intensity and few m/z signals at 35% (v/v) ACN (see Fig. 3A). However, a substantial peptide spectrum was obtained from the correlative supernatants after digestion as shown in Fig. 3B. Therefore, we decided to profile through

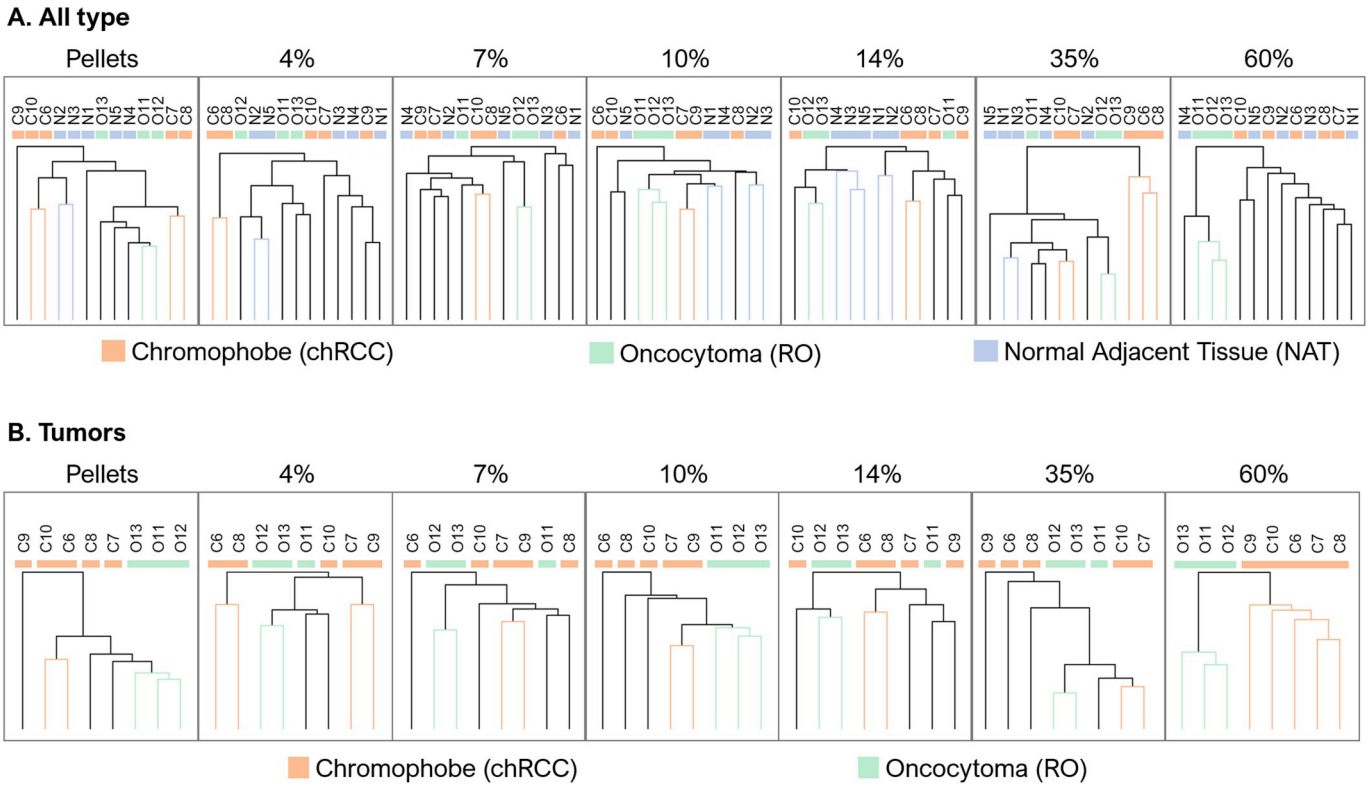

Fig. 4. Unsupervised clustering analysis of MALDI-based mass spectrometry data obtained for peptides from (i) the digested pellets and (ii) sequentially eluted fractions from the digested supernatants using C18 tips and 4%, 7%, 10%, 14%, 35% and 60% (v/v) of ACN. Clusters obtained (A) using the three types of solid biopsies, chromophobe, oncocytoma and NAT and (B) using only data from chromophobe and oncocytoma. For the latest case note the 60% ACN (v/v) concentration.

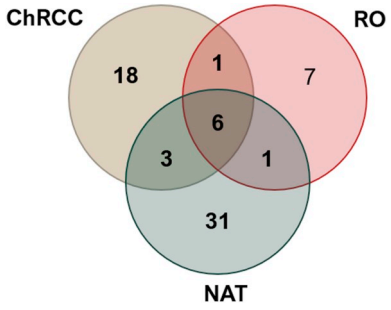

Fig. 5. Venn diagram (n_{chRCC} = 5, n_{RO} = 3, n_{NAT} = 5) showing the number of proteins identified for the 60% ACN supernatant fraction by nano-LC-HR-MS/MS. Proteins are listed in Fig. 6.

a MALDI-MS approach the supernatants using the sequential extraction approach while interrogating the complete protein content of the pellets.

Quintuple MALDI spectra were obtained for each fraction. The cohorts of m/z signals were used to analyze the samples by unsupervised clustering. The results showed that classification of the chRCC, RO and NAT samples clustered together was not possible at any of the ACN extracting concentrations tested as shown in Fig. 4A. The best classification was obtained for the oncocytoma samples that were grouped using the cohorts of m/z signals obtained for the ACN concentrations (v/v) of 10% and 60%. It is noteworthy that the clustering using the pellets protein content of the pellets also failed in classifying the samples as may be seen in Fig. 4A. However, comparing only the oncocytoma and chromophobe biopsies without NAT biopsies showed excellent discrimination using the cohorts of m/z signals obtained for the ACN extraction at a concentration of 60% (v/v) (see Fig. 4B, panel 7).

3.3. Revealing the protein content of the optimal extraction fraction

These data indicated that the pool of peptides obtained with 60% ACN (v/v) concentration was most informative in distinguishing between the renal tumor classifications. The entire preparation protocol was repeated using the original samples to obtain peptides from the ACN 60% fraction for analysis in the nano-LC-HR-MS. Eighteen proteins specific to chRCC and seven unique to RO were found based on this approach (see Fig. 5).

The chromophobe tumors expressed 5 proteins associated with canonical ATP function (ATP5I & 5E; VATE1 & G2; ADT2) and one classical glycolytic enzyme (PGK1). In addition, neuromedin was detected specific to the chromophobe tumors. It is interesting to note that changes in the function or expression of these molecules has been previously reported in renal [22–24], pancreatic [25,26] and lung [25] cancers. Oncocytomas expressed ATP5H and ATPA, DEPD7 and TRIPB (thyroid receptor interacting protein). It is noteworthy that both, oncocytoma and chromophobe are characterized by an eosinophilic cytoplasm which contains excessive amounts of mitochondria [27–31]. In the case of the chromophobe pathology, 5 of the proteins we detected were related to mitochondrial function while two ATP-related proteins were found specific to the oncocytomas. The complete list of proteins is presented in Fig. 6.

4. Concluding remarks

We have developed a method using ultrasonic energy in conjunction with fast C18 tips sequential extraction and MALDI-snapshotting that is capable of delineating the complex proteomes from solid biopsies of chromophobe renal cell carcinoma and renal oncocytomas. It is also possible to obtain unsupervised clustering of these solid biopsies with optimal discrimination of the chromophobe and oncocytoma specimens using the 60% ACN extraction procedure. This approach yielded 18

Accession	Protein	MW [kDa]	pI	ChRCC	RO	NAT
H2B1K_HUMAN	Histone H2B type 1-K	13.9	10.3	■	■	■
H4_HUMAN	Histone H4	11.4	11.4	■	■	■
HBA_HUMAN	Hemoglobin subunit alpha	15.2	8.7	■	■	■
HBB_HUMAN	Hemoglobin subunit beta	16.0	6.7	■	■	■
HSPB1_HUMAN	Heat shock protein beta-1	22.8	6.0	■	■	■
VIME_HUMAN	Vimentin	53.6	5.1	■	■	■
ACTB_HUMAN	Actin, cytoplasmic 1	41.7	5.3	■		■
COF1_HUMAN	Cofilin-1	18.5	8.2	■		■
ENOA_HUMAN	Alpha-enolase	47.1	7.0	■		■
KCRB_HUMAN	Creatine kinase B-type	42.6	5.3	■		■
VTNC_HUMAN	Vitronectin	54.3	5.6		■	■
ACTG_HUMAN	Actin, cytoplasmic 2	41.8	5.3		■	■
ADT2_HUMAN	ADP/ATP translocase 2	32.9	9.8	■		
AK1A1_HUMAN	Alcohol dehydrogenase [NADP+]	36.5	6.3			■
AL4A1_HUMAN	Delta-1-pyrroline-5-carboxylate dehydrogenase, mitochondrial	61.7	8.2			■
ALBU_HUMAN	Serum albumin	69.3	5.9			■
ALDOB_HUMAN	Fructose-bisphosphate aldolase B	39.4	8.0			■
ARHGC_HUMAN	Rho guanine nucleotide exchange factor 12	173.1	5.5	■		
ATP5E_HUMAN	ATP synthase subunit epsilon, mitochondrial	5.8	9.9	■		
ATP5H_HUMAN	ATP synthase subunit d, mitochondrial	18.5	5.2		■	
ATP5I_HUMAN	ATP synthase subunit e, mitochondrial	7.9	9.3	■		
ATPA_HUMAN	ATP synthase subunit alpha, mitochondrial	59.7	9.2		■	
BTBD3_HUMAN	BTB/POZ domain-containing protein 3	58.4	7.4			■
CALD1_HUMAN	Caldesmon	93.2	5.6			■
CATB_HUMAN	Cathepsin B	37.8	5.9			■
CH60_HUMAN	60 kDa heat shock protein, mitochondrial	61.0	5.7	■		
CND3_HUMAN	Condensin complex subunit 3	114.3	5.4			■
DEN4B_HUMAN	DENN domain-containing protein 4B	163.7	6.9			■
DEPD7_HUMAN	DEP domain-containing protein 7	58.3	7.6		■	
EZRI_HUMAN	Ezrin	69.4	5.9			■
FA5_HUMAN	Coagulation factor V	251.5	5.7	■		
GP123_HUMAN	Probable G-protein coupled receptor 123	137.1	9.2			■
H12_HUMAN	Histone H1.2	21.4	10.9			■
H14_HUMAN	Histone H1.4	21.9	11.0			■
H2A1H_HUMAN	Histone H2A type 1-H	13.9	10.9			■
H2AV_HUMAN	Histone H2A.V	13.5	10.6		■	
HPS5_HUMAN	Hermansky-Pudlak syndrome 5 protein	127.4	5.4			■
IF122_HUMAN	Intraflagellar transport protein 122 homolog	141.7	6.1		■	
IGKC_HUMAN	Ig kappa chain C region	11.6	5.6			■
K1C18_HUMAN	Keratin, type I cytoskeletal 18	48.0	5.3	■		
M2OM_HUMAN	Mitochondrial 2-oxoglutarate/malate carrier protein	34.0	9.9	■		
MAP4_HUMAN	Microtubule-associated protein 4	120.9	5.3	■		
MISSL_HUMAN	MAPK-interacting and spindle-stabilizing protein-like	24.3	5.3	■		
MLL1_HUMAN	Histone-lysine N-methyltransferase MLL	431.5	9.2			■
MSH2_HUMAN	DNA mismatch repair protein Msh2	104.7	5.6			■
NHRF1_HUMAN	Na(+)/H(+) exchange regulatory cofactor NHE-RF1	38.8	5.6			■
NMU_HUMAN	Neuromedin-U	19.7	9.1	■		
NOL11_HUMAN	Nucleolar protein 11	81.1	5.7			■
NOTC2_HUMAN	Neurogenic locus notch homolog protein 2	265.2	5.0			■
PEBP1_HUMAN	Phosphatidylethanolamine-binding protein 1	21.0	7.0			■
PGK1_HUMAN	Phosphoglycerate kinase 1	44.6	8.3	■		
PPIA_HUMAN	Peptidyl-prolyl cis-trans isomerase A	18.0	7.7	■		
PSMD2_HUMAN	26S proteasome non-ATPase regulatory subunit 2	100.1	5.1			■
PTMA_HUMAN	Prothymosin alpha	12.2	3.7			■
PTMS_HUMAN	Parathymosin	11.5	4.1			■
QCR6_HUMAN	Cytochrome b-c1 complex subunit 6, mitochondrial	10.7	4.4		■	
RADIL_HUMAN	Ras-associating and dilute domain-containing protein	117.4	6.7			■
SMBP2_HUMAN	DNA-binding protein SMUBP-2	109.1	9.1	■		
TARA_HUMAN	TRIO and F-actin-binding protein	261.2	8.9			■
TBA1C_HUMAN	Tubulin alpha-1C chain	49.9	5.0			■
TPM4_HUMAN	Tropomyosin alpha-4 chain	28.5	4.7			■
TRIPB_HUMAN	Thyroid receptor-interacting protein 11	227.5	5.2		■	
TSTD1_HUMAN	Thiosulfate sulfurtransferase/rhodanese-like domain-containing protein 1	12.5	5.9			■
USMG5_HUMAN	Up-regulated during skeletal muscle growth protein 5	6.5	9.8	■		
VATE1_HUMAN	V-type proton ATPase subunit E 1	26.1	7.7	■		
VATG2_HUMAN	V-type proton ATPase subunit G 2	13.6	10.3	■		
VDAC1_HUMAN	Voltage-dependent anion-selective channel protein 1	30.8	8.6	■		

Fig. 6. List of proteins identified for the chRCC, RO and NAT solid biopsies in the fraction eluted from the C18 tips using the ACN 60% (v/v) solution. Grey colored boxes indicate the presence of the protein.

proteins unique to chromophobe renal cell carcinoma versus 7 unique to oncocytoma, from a total of 67 proteins found in the fraction of interest. The proposed method is fast, simple and low-cost, and therefore ideal for efficient analysis of solid biopsies. The most informative extracts can be easily identified for further analysis by HR-MS to obtain deep knowledge of a large number of individual features. The method proposed last 14 h for one sample, from the beginning of the sample treatment to the MALDI analysis. However, with the high throughput provided by the 96-well plate-based ultrasonic approach [12], the total time needed would be reduced from 14 h per sample to 96 samples in 14 h, this is approx. 9 min per sample. This approach holds the promise of discriminating between an indolent renal neoplasms and aggressive kidney tumors that are otherwise difficult to classify using current immunocytochemical methods and could have an impact on the diagnosis and therapy of these patients.

Conflicts of interest

All authors declare no competing interests.

Acknowledgements

PROTEOMASS Scientific Society is acknowledged by the funding provided to the Laboratory for Biological Mass Spectrometry Isabel Moura. Authors acknowledge the funding provided by the Associate Laboratory for Green Chemistry LAQV which is financed by national funds from FCT/MEC (UID/QUI/50006/2019). H. M. S. is funded by the FCT 2015 Investigator Program (IF/00007/2015). S. J. thanks FCT/MEC (Portugal) for her research contract as PhD student with the grant SFRH/BD/120537/2016. J.F.L. Acknowledges FCT/MEC (Portugal) SFRH/BPD/93982/2013 and FCT-UNL for the DL57/2016 Assistant Researcher Contract. H. López-Fernández is supported by a post-doctoral fellowship from Xunta de Galicia (ED481B 2016/068-0). This project utilized the University of Pittsburgh Hillman Cancer Center shared resource facility (Cancer Genomics Facility) supported in part by award P30CA047904 (Dr. LaFramboise).

Appendix A. Supplementary data

Supplementary data to this article can be found online at https://doi.org/10.1016/j.talanta.2019.120180.

References

[1] N.J. Farber, C.J. Kim, P.K. Modi, J.D. Hon, E.T. Sadimin, E.A. Singer, Renal cell carcinoma: the search for a reliable biomarker, Transl. Cancer Res. 6 (2017) 620–632, https://doi.org/10.21037/tcr.2017.05.19.
[2] S. Jain, S. Roy, M. Amin, M. Acquafondata, M. Yin, W. Laframboise, S. Bastacky, L. Pantanowitz, R. Dhir, A. Parwani, Amylase α-1A (AMY1A): a novel immunohistochemical marker to differentiate chromophobe renal cell carcinoma from benign oncocytoma, Am. J. Surg. Pathol. 37 (2013) 1824–1830, https://doi.org/10.1097/PAS.0000000000000108.
[3] A.M. Badowska-Kozakiewicz, M.P. Budzik, P. Koczkodaj, J. Przybylski, Selected tumor markers in the routine diagnosis of chromophobe renal cell carcinoma, Arch. Med. Sci. 12 (2016) 856–863, https://doi.org/10.5114/aoms.2015.51188.
[4] S. Huang, G. Chen, N. Ye, X. Kou, F. Zhu, J. Shen, G. Ouyang, Solid-phase microextraction: an appealing alternative for the determination of endogenous substances - a review, Anal. Chim. Acta (2019), https://doi.org/10.1016/J.ACA.2019.05.054.
[5] R. Venson, A.-S. Korb, G. Cooper, A review of the application of hollow-fiber liquid-phase microextraction in bioanalytical methods – a systematic approach with focus on forensic toxicology, J. Chromatogr. B 1108 (2019) 32–53, https://doi.org/10.1016/J.JCHROMB.2019.01.006.
[6] H. Tabani, S. Nojavan, M. Alexovič, J. Sabo, Recent developments in green membrane-based extraction techniques for pharmaceutical and biomedical analysis, J. Pharm. Biomed. Anal. 160 (2018) 244–267, https://doi.org/10.1016/J.JPBA.2018.08.002.
[7] M. Alexovič, Y. Dotsikas, P. Bober, J. Sabo, Achievements in robotic automation of solvent extraction and related approaches for bioanalysis of pharmaceuticals, J. Chromatogr. B 1092 (2018) 402–421, https://doi.org/10.1016/J.JCHROMB.2018.06.037.
[8] M. Ahmadi, H. Elmongy, T. Madrakian, M. Abdel-Rehim, Nanomaterials as sorbents for sample preparation in bioanalysis: a review, Anal. Chim. Acta 958 (2017) 1–21, https://doi.org/10.1016/J.ACA.2016.11.062.
[9] C.E.D. Nazario, B.H. Fumes, M.R. da Silva, F.M. Lanças, New materials for sample preparation techniques in bioanalysis, J. Chromatogr. B 1043 (2017) 81–95, https://doi.org/10.1016/J.JCHROMB.2016.10.041.
[10] J.A. Ocaña-González, R. Fernández-Torres, M.Á. Bello-López, M. Ramos-Payán, New developments in microextraction techniques in bioanalysis. A review, Anal. Chim. Acta 905 (2016) 8–23, https://doi.org/10.1016/J.ACA.2015.10.041.
[11] C. Fernández-costa, M. Reboiro-jato, F. Fdez-riverola, C. Ruiz-romero, F.J. Blanco, J.-L. Capelo-martínez, Sequential depletion coupled to C18 sequential extraction as a rapid tool for human serum multiple profiling, Talanta 125 (2014) 189–195, https://doi.org/10.1016/j.talanta.2014.02.050.
[12] S. Jorge, J.E. Araújo, F.M. Pimentel-santos, J.C. Branco, H.M. Santos, C. Lodeiro, J.L. Capelo, Unparalleled sample treatment throughput for proteomics workflows relying on ultrasonic energy, Talanta 178 (2018) 1067–1076, https://doi.org/10.1016/j.talanta.2017.07.079.
[13] C. Fernández, H.M. Santos, C. Ruíz-Romero, F.J. Blanco, J.-L. Capelo-Martínez, A comparison of depletion versus equalization for reducing high-abundance proteins in human serum, Electrophoresis 32 (2011) 2966–2974, https://doi.org/10.1002/elps.201100183.
[14] C. Fernández-Costa, V. Calamia, P. Fernández-Puente, J.-L. Capelo-Martínez, C. Ruiz-Romero, F.J. Blanco, Sequential depletion of human serum for the search of osteoarthritis biomarkers, Proteome Sci. 10 (2012) 1–12, https://doi.org/10.1186/1477-5956-10-55.
[15] J. Rappsilber, Y. Ishihama, M. Mann, Stop and Go Extraction tips for matrix-assisted laser desorption/ionization, nanoelectrospray, and LC/MS sample pretreatment in proteomics, Anal. Chem. 75 (2003) 663–670, https://doi.org/10.1021/ac026117i.
[16] S. Jorge, J.L. Capelo, W. LaFramboise, R. Dhir, C. Lodeiro, H.M. Santos, Development of a robust ultrasonic-based sample treatment to unravel the proteome of OCT-embedded solid tumor biopsies, J. Proteome Res. 18 (2019) 2979–2986, https://doi.org/10.1021/acs.jproteome.9b00248.
[17] G. Martins, J. Fernández-Lodeiro, J. Djafari, C. Lodeiro, J.L. Capelo, H.M. Santos, Label-free protein quantification after ultrafast digestion of complex proteomes using ultrasonic energy and immobilized-trypsin magnetic nanoparticles, Talanta 196 (2019) 262–270, https://doi.org/10.1016/j.talanta.2018.12.066.
[18] K. Atacan, B. Çakıroğlu, M. Özacar, Efficient protein digestion using immobilized trypsin onto tannin modified Fe3O4magnetic nanoparticles, Colloids Surfaces B Biointerfaces 156 (2017) 9–18, https://doi.org/10.1016/j.colsurfb.2017.04.055.
[19] L. Zhang, B. Wang, S. Wang, W. Zhang, Recyclable trypsin immobilized magnetic nanoparticles based on hydrophilic polyethylenimine modification and their proteolytic characteristics, Anal. Methods. 10 (2018) 459–466, https://doi.org/10.1039/c7ay02418e.
[20] H. Lopez-Fernandez, H.M. Santos, J.L. Capelo, F. Fdez-Riverola, D. Glez-Pena, M. Reboiro-Jato, Mass-Up: an all-in-one open software application for MALDI-TOF mass spectrometry knowledge discovery, BMC Bioinf. 16 (2015), https://doi.org/10.1186/s12859-015-0752-4.
[21] J. Prates, G. Martins, H. López-fernández, C. Lodeiro, Talanta Modulating the protein content of complex proteomes using acetonitrile, Talanta 182 (2018) 333–339, https://doi.org/10.1016/j.talanta.2018.01.057.
[22] G. Solaini, G. Sgarbi, A. Baracca, Oxidative phosphorylation in cancer cells, Biochim. Biophys. Acta Bioenerg. 1807 (2011) 534–542, https://doi.org/10.1016/j.bbabio.2010.09.003.
[23] A. Chevrollier, D. Loiseau, P. Reynier, G. Stepien, Adenine nucleotide translocase 2 is a key mitochondrial protein in cancer metabolism, Biochim. Biophys. Acta Bioenerg. 1807 (2011) 562–567, https://doi.org/10.1016/j.bbabio.2010.10.008.
[24] S.K. Harten, M.A. Esteban, D. Shukla, M. Ashcroft, P.H. Maxwell, Inactivation of the von Hippel-Lindau tumour suppressor gene induces Neuromedin U expression in renal cancer cells, Mol, Cancer 10 (2011) 1–7, https://doi.org/10.1186/1476-4598-10-89.
[25] L. Stransky, K. Cotter, M. Forgac, The function of V-ATPases in cancer, Physiol. Rev. 96 (2016) 1071–1091, https://doi.org/10.1152/physrev.00035.2015.
[26] T.-L. Hwang, Y. Liang, K.-Y. Chien, J.-S. Yu, Overexpression and elevated serum levels of phosphoglycerate kinase 1 in pancreatic ductal adenocarcinoma, Proteomics 6 (2006) 2259–2272, https://doi.org/10.1002/pmic.200500345.
[27] S. Joshi, D. Tolkunov, H. Aviv, A.A. Hakimi, M. Yao, J.J. Hsieh, S. Ganesan, C.S. Chan, E. White, The genomic landscape of renal oncocytoma identifies a metabolic barrier to tumorigenesis, Cell Rep. 13 (2015) 1895–1908, https://doi.org/10.1016/j.celrep.2015.10.059.
[28] G. Gasparre, G. Romeo, M. Rugolo, A.M. Porcelli, Learning from oncocytic tumors: Why choose inefficient mitochondria? Biochim. Biophys. Acta Bioenerg. 1807 (2011) 633–642, https://doi.org/10.1016/J.BBABIO.2010.08.006.
[29] K.W. Rathmell, F. Chen, C.J. Creighton, Genomics of chromophobe renal cell carcinoma: implications from a rare tumor for pan-cancer studies, Oncoscience 2 (2015) 81–90, https://doi.org/10.18632/oncoscience.130.
[30] S.H. Yun, E.C. Park, S.Y. Lee, H. Lee, C.W. Choi, Y.S. Yi, H.J. Ro, J.C. Lee, S. Jun, H.Y. Kim, G.H. Kim, S. Il Kim, Antibiotic treatment modulates protein components of cytotoxic outer membrane vesicles of multidrug-resistant clinical strain, Acinetobacter baumannii DU202, Clin. Proteonomics 15 (2018), https://doi.org/10.1186/s12014-018-9204-2.
[31] W. Lee, Imprint cytology of the chromophobe renal cell carcinoma: Correlation with the histological and ultrastructural features, J. Cytol. 28 (2011) 77–80, https://doi.org/10.4103/0970-9371.80749.